High-resolution quantification of atmospheric CO_2 mixing ratios in the Greater Toronto Area, Canada

Stephanie C. Pugliese[a], Jennifer G. Murphy[a*], Felix R. Vogel[b,d], Michael D. Moran[c], Junhua Zhang[c], Qiong Zheng[c], Craig A. Stroud[c], Shuzhan Ren[c], Douglas Worthy[d], Gregoire Broquet[b]

[a] University of Toronto, Department of Chemistry, 80 St. George St, Toronto, ON, Canada M5S 3H6

[b] Laboratoire des Sciences du Climat et de L'Environnement, CEA-CNRS-UVSQ, Université de Paris-Saclay, France

[e]Environment and Climate Change Canada, Air Quality Research Division, 4905 Dufferin St. Toronto, ON, Canada M3H 5T4

[d] Environment and Climate Change Canada, Climate Research Division, 4905 Dufferin St. Toronto, ON, Canada M3H 5T4

*Correspondence to: Jennifer G. Murphy (jmurphy@chem.utoronto.ca)

Abstract

Many stakeholders are seeking methods to reduce carbon dioxide (CO_2) emissions in urban areas, however reliable, high-resolution inventories are required to guide these efforts. We present the development of a high-resolution CO_2 inventory available for the Greater Toronto Area and surrounding region in southern Ontario, Canada (area of ~2.8×10^5 km^2, 26 % of the province of Ontario). The new SOCE (Southern Ontario CO_2 Emissions) inventory is available at the 2.5 x 2.5 km spatial and hourly temporal resolution and characterizes emissions from seven sectors: Area, Residential natural gas combustion, Commercial natural gas combustion, Point, Marine, On-road and Off-road. To assess the accuracy of the SOCE inventory, we developed an observation-model framework using the GEM-MACH chemistry-transport model run on a high-resolution grid with 2.5 km grid spacing coupled to the Fossil Fuel Data Assimilation System (FFDAS) v2 inventories for anthropogenic CO_2 emissions and the European Center for Medium-Range Weather Forecasts (ECMWF) land carbon model C-TESSEL for biogenic fluxes. A run using FFDAS for the southern Ontario region was compared to a run in which its emissions were replaced by the SOCE inventory. Simulated CO_2 mixing ratios were compared against in situ measurements made at four sites in southern Ontario, Downsview, Hanlan's Point, Egbert and Turkey Point, in three winter months, January-March, 2016. Model simulations had better agreement with measurements when using the SOCE inventory emissions versus other inventories, quantified using a variety of statistics such as Correlation Coefficient, root mean square error and mean bias. Furthermore, when run with the SOCE inventory, the model had improved ability to capture the typical diurnal pattern of CO_2 mixing ratios, particularly at the Downsview, Hanlan's Point and Egbert sites. In addition to improved model-measurement agreement, the SOCE inventory offers a sectoral breakdown of emissions, allowing estimation of average time-of-day and day-of-week contributions of different sectors. Our results show that at night, emissions from Residential and Commercial natural gas combustion and

other Area sources can contribute > 80 % of the CO_2 enhancement while during the day emissions from the On-road sector dominate, accounting for >70 % of the enhancement.

1.0 Introduction

Urban areas are sites of dense population and the intensity of human activities (such as transportation, industry and residential and commercial development) makes them hot-spots for anthropogenic carbon dioxide (CO_2) emissions. While occupying only 3 % of the total land area, urban areas are locations of residence for 54 % of the global population and are the source of 53 – 87 % of anthropogenic CO_2 emissions globally (IPCC-WG3, 2014; WHO, 2015). When considering Canada alone, the urban population accounts for an even larger fraction of the total (81 % in 2011) (Statistics Canada, 2011) while urban areas cover only 0.25 % of the land area (Statistics Canada, 2009). Recognizing their influence on the global carbon budget, many urban areas are seeking methods to reduce their anthropogenic CO_2 emissions. The Greater Toronto Area (GTA) in southeastern Canada, for example, has committed to the *Change is in the Air* initiative as well as being a part of the *C40 Cities Climate Leadership Group,* both of which call to reduce CO_2 emissions 30 % below 1990 levels by 2020 (C40 Cities, 2016; Framework for Public Review and Engagement, 2007). However, in order to effectively guide anthropogenic CO_2 mitigation strategies, reliable inventories are needed, particularly at high spatial and temporal resolution, to gain a better understanding of the carbon cycle (Gurney et al., 2009; Patarasuk et al., 2016). To our knowledge, the only spatially disaggregated CO_2 inventories available for use in the GTA are the EDGAR v.4.2 (Emission Database for Global Atmospheric Research) CO_2 inventory (available at annual, 0.1^o x 0.1^o resolution) (EDGAR, 2010) and the FFDAS v2 (Fossil Fuel Data Assimilation System) CO_2 inventory (available at hourly, 0.1^o x 0.1^o resolution) (FFDAS, 2010), both which are limited in their spatial and/or temporal resolution and therefore are not well-suited for the quantification and

62 understanding of CO_2 emissions at the urban scale. The Canadian national CO_2 inventory, on the
63 other hand, is only available at the provincial level (Environment Canada, 2012).

64 Efforts to develop emission inventories at the fine spatial and temporal resolution required
65 for urban-scale understanding of CO_2 emissions has been driven both by policy- and science-related
66 questions (Gurney et al., 2009; Patarasuk et al., 2016). From a policy perspective, improving CO_2
67 emission quantification is essential to independently evaluate whether anthropogenic mitigation
68 regulations are being effectively implemented. From a scientific perspective, gaining information
69 about anthropogenic CO_2 emissions from urban areas has been primarily motivated by atmospheric
70 CO_2 inversions, which are used to better understand the global carbon cycle (Gurney et al., 2009;
71 Patarasuk et al., 2016). Regardless of the motivation, quantification of CO_2 source/sink processes
72 currently uses two techniques: the bottom-up approach and the top-down approach. In the bottom-
73 up approach, local-scale activity level information is combined with appropriate emission factors to
74 infer emission rates. This method has been used widely to develop many inventories (EDGAR,
75 2010; FFDAS, 2010; Gurney et al., 2009) but is limited by the accuracy of the input parameters.
76 Conversely, in the top-down approach, inverse modelling is used to exploit the variability in
77 atmospheric mixing ratios of CO_2 to identify the source/sink distributions and magnitudes; this
78 method is limited by insufficient mixing ratio data and uncertainties in simulating atmospheric
79 transport (Pillai et al., 2011). Given current policy needs, a strategy using solely bottom-up or top-
80 down approaches is likely insufficient to evaluate CO_2 emissions but rather a synthesis of the two
81 methodologies is required (Miller and Michalak, 2016). Successful examples of high-resolution CO_2
82 inventory development are available on the urban scale, such as the Airparif inventory in Ile-de-
83 France (publicly available at http://www.airparif.asso.fr/en/index/index) and in Indianapolis, Los
84 Angeles, Salt Lake City and Phoenix through the Hestia project (Gurney et al., 2012), on the national
85 scale, such as in China (Zhao et al., 2012), and on the global scale (Wang et al., 2013). However, to

our knowledge, there are currently no studies that have quantified Canadian CO_2 emissions at the fine spatial and temporal resolution required for urban analyses in Canada.

In an effort to address this gap, this study was focused on quantifying CO_2 emissions at a fine spatial and temporal resolution in the GTA and southern Ontario (we expanded the inventory beyond the urban area of the GTA so we could exploit information on CO_2 mixing ratios collected at rural areas in central and south-western Ontario, proving additional sites for inventory validation). We present the new high-resolution Southern Ontario CO_2 Emissions (SOCE) inventory, which quantifies CO_2 emissions from seven source sectors (On-road, Off-road, Area, Point, Marine, Residential, and Commercial natural gas combustion) at 2.5 km x 2.5 km spatial and hourly temporal resolution for an area covering ~26 % of the province of Ontario (~2.8×10^5 km^2). The SOCE inventory was used in combination with the Environment and Climate Change Canada (ECCC) GEM-MACH chemistry-transport model to simulate CO_2 mixing ratios in a domain including south-eastern Canada and the northeastern USA (hereafter referred to as the "PanAm domain") for comparison with in situ measurements made by the Southern Ontario Greenhouse Gas Network. Until now, estimates of anthropogenic CO_2 emissions in the GTA were available only from the EDGAR v.4.2 (EDGAR, 2010) and the FFDAS v2 (FFDAS, 2010) inventories, which have very different annual totals for this region (1.36×10^8 vs. 1.05×10^8 tonnes CO_2, respectively). Therefore, we expect the results of this work will improve our ability to quantify the emissions of CO_2 in the entire domain as well as the relative contributions of different sectors, providing a more detailed characterization of the carbon budget in the GTA.

2.0 Methods

2.1 Geographic Domain

The geographic focus of this study was the GTA in southern Ontario, Canada. The GTA is the largest urban area in Canada; it comprises five municipalities, Toronto, Halton, Durham, Peel and York,

which together have a population exceeding 6 million (Statistics Canada., 2012b). Although the GTA comprises only 0.07 % of Canadian land area, it represents over 17 % of the total population as a result of rapid urbanization over the past few decades (Statistics Canada., 2012b). Therefore, high-resolution characterization of CO_2 emissions can help integrate climate policy with urban planning. This region is home to a network of measurement sites providing long-term, publicly available datasets of atmospheric CO_2 mixing ratio measurements, *Section 2.2* (Environment Canada, 2011) which can be used to evaluate model outputs and inventory estimates. In 2016 the government of Ontario released a Climate Change Action Plan, which includes an endowment given to the Toronto Atmospheric Fund of $17 million to invest in strategies to reduce greenhouse gas pollution in the GTA (Ontario, 2016). Therefore this research can provide timely information on the carbon budget in the GTA and help to implement effective reduction strategies.

2.2 The Southern Ontario Greenhouse Gas Network

Measurements of ambient CO_2 dry air mixing ratios began in 2005 in southern Ontario at the Egbert station followed by the Downsview station (2007), Turkey Point station (2012) and Hanlan's Point station (2014), Figure 1. Measurements were also temporarily made at a site in downtown Toronto, the Toronto Atmospheric Observatory (TAO) (43.7°N, 79.4°W), but the instrument was relocated from this site in January 2016. Egbert is located ~75 km north-northwest of Toronto in a rural area, Downsview is located ~20 km north of downtown core of the city of Toronto in a populated suburban area, Turkey Point is located to the south-west of the GTA in a rural area on the north shore of Lake Erie, and Hanlan's Point is located on Toronto Island, just south of the city of Toronto on the shore of Lake Ontario. Site details and instrument types used can be found in Table 1. CO_2 measurements are collected as a part of ECCC's Greenhouse Gas Observational Program. The measurement procedure follows a set of established principles and protocols outlined by a number of international agencies through recommendations of the *Meeting on Carbon Dioxide, Other*

134 *Greenhouse Gases, and Related Measurement Techniques,* coordinated by the World Meteorological
135 Organization (WMO) every 2 years.

136 The atmospheric CO_2 observational program at the Egbert site is based on non-dispersive
137 infrared (NDIR) methodology and fine-tuned for high precision measurements (Worthy et al.,
138 2005). A detailed description of the NDIR observational system can be found in Worthy et al,
139 (2005). The atmospheric CO_2 observational programs at Turkey Point, Downsview, and Hanlan's
140 Point are based on Cavity Ring-Down Spectrometer (CRDS). Each Picarro CRDS system is calibrated
141 in the ECCC central calibration facility in Toronto before deployment to the field. The response
142 function of the analyzer is determined against 3 calibrated standards tanks (Low, Mid, High). The
143 working (W) and target (T) tanks assigned to the system are also included in the injection sequence
144 and calibrated. At each site, ambient measurements are made using two sample lines placed at the
145 same level. Each sample line has separate dedicated sample pumps and driers (~ -30^{o}C).
146 Pressurized aluminum 30 L gas cylinders are used for the working and target tanks. The sample
147 flow rate of the ambient and standard tank gases is set at ~300 cc/min. The injection sequence
148 consists of a target and working tanks sequentially passed through the analyzer for 10 minutes
149 each every 2 days. The ambient data from line1 is passed through the analyzer for 18 hours
150 followed by Line2 for 6 hours. The Line1/Line2 sequence repeats one time before the target and
151 working tanks are again passed through the system. The working and target tanks are calibrated on
152 site at least once per year against a single transfer standard transported between the sites and the
153 central laboratory facility in Toronto. The CO_2 measurements from both the NDIR and CRDS
154 analytical systems have a precision of around 0.1 ppm based on one-minute averages and are
155 accurate to within 0.2 ppm.

156

157

158 *2.3 GEM-MACH chemistry- transport model*

159 In this project, we used the GEM-MACH (Global Environmental Multi-scale–Modelling Air quality
160 and CHemistry) chemistry–transport model (CTM) (Gong et al., 2015; Moran et al., 2013; Pavlovic
161 et al., 2016; Talbot et al., 2008) to link surface emission estimates and atmospheric mixing ratios.
162 GEM-MACH is an on–line CTM embedded within the Canadian weather forecast model GEM (Côté et
163 al., 1998a; Côté et al., 1998b). The configuration of GEM-MACH used in our study has 62 vertical
164 levels from the surface to ~1.45 hPa on a terrain-following staggered vertical grid for a log-
165 hydrostatic pressure coordinate. The thickness of the lowest layer was 40 m. The PanAm domain
166 used in our simulations, which includes central and southern Ontario, as well as western Quebec
167 and the northeastern USA, is shown in Figure 1. The PanAm domain has 524 x 424 grid cells in the
168 horizontal on a rotated latitude-longitude grid with 2.5-km grid spacing and covers an area of
169 approximately 1310 km x 1060 km (total domain area is 1.39×10^6 km^2). A 24-hour forecasting
170 period was used with a 60-second time step for each integration cycle. Meteorological fields (wind,
171 temperature, humidity, etc.) were re-initialized every 24 hours (i.e., after each model integration
172 cycle); chemical fields were carried forward from the previous integration cycle (i.e., perpetual
173 forecast). Hourly meteorological and chemical boundary conditions were provided by the ECCC
174 operational 10-km GEM-MACH air quality forecast model (Moran et al., 2015).

175 In our study, we simulated two scenarios of CO_2 surface fluxes, indicated by the sum of the
176 following:

177 Scenario 1:

178 • Anthropogenic fossil fuel CO_2 emissions within the province of Ontario estimated by the
179 SOCE inventory, available at 2.5 km x 2.5 km spatial and hourly temporal resolution, as
180 described in *Section 2.4*

- Anthropogenic fossil fuel CO_2 emissions estimated by the FFDAS v2 inventory (FFDAS, 2010) outside of the province of Ontario (province of Quebec and USA), available at 0.1^o x 0.1^o spatial and hourly temporal resolution
- Biogenic CO_2 fluxes from the C-TESSEL land surface model, as described in *Section 2.5*

Scenario 2:

- Anthropogenic fossil fuel CO_2 emissions estimated by the FFDAS v2 inventory (FFDAS, 2010) for the entire domain, available at 0.1^o x 0.1^o spatial and hourly temporal resolution
- Biogenic CO_2 fluxes from the C-TESSEL land surface model, as described in *Section 2.5*

CO_2 is not a usual chemical species considered by GEM-MACH but a set of special inert tracer fields were added to GEM-MACH for this project to account for CO_2 concentration fields associated with difference source sectors and the lateral boundaries. The CO_2 boundary conditions set at the lateral and top edges of the domain were obtained from the Monitoring Atmospheric Composition and Climate (MACC) global inversion, v.10.2 (http://www.copernicus-atmosphere.eu/). Model simulated specific humidity (q, kg/kg) was used to convert estimated CO_2 mixing ratios to dry air mixing ratios. CO_2 dry air mixing ratios are hereafter referred to CO_2 mixing ratios.

2.4 High-Resolution SOCE inventory development

The high-resolution SOCE inventory was constructed primarily from a pre-existing carbon monoxide (CO) inventory developed by the Pollutant Inventories and Reporting Division (PIRD) of ECCC as part of the 2010 Canadian Air Pollutant Emissions Inventory (APEI). The CO inventory is a comprehensive national anthropogenic inventory that includes emissions from area sources, point sources, on-road mobile sources and off-road mobile sources, including aircraft, locomotive and marine emissions for base year 2010 (Moran et al., 2015). This annual inventory at the provincial level compiled by PIRD was transformed into model-ready emissions files using the Sparse Matrix

Operator Kernel Emissions (SMOKE, https://www.cmascenter.org/smoke/) emissions processing system for spatial allocation (distribution of non-point source emissions to 2.5 km x 2.5 km (roughly 0.02^o x 0.02^o resolution) using spatial surrogate fields) and temporal allocation (conversion of inventory annual emission rates into hourly values) (Moran et al., 2015). Because Ontario CO emissions in the 2010 APEI were processed in separate steps with SMOKE by primary source sector, files of gridded hourly CO emissions fields were available for seven different inventory sectors: area sources; point sources; on-road mobile sources; off-road mobile sources; marine sources; residential natural-gas sources; and commercial natural-gas sources. The spatial and temporal allocations applied to these seven sectors were different, so in effect they constitute a set of spatiotemporal emissions basis functions. More detailed information about the CO inventory compilation and subsequent processing has been provided elsewhere (Environment Canada, 2013; Moran et al., 2015; PIRD, 2016).

The objective of our work was to calculate CO_2 emissions based on this processed, sector-specific, model-ready CO inventory for Ontario grid cells using sector-specific emission ratios estimated by the Canadian National Inventory Report (NIR) (Environment Canada, 2012). The NIR estimates CO_2 and CO emissions using primarily bottom-up estimates; for example, emissions from industrial process are estimated using production data reported directly by facilities whereas emissions from road transport activities are estimated using vehicle population data, fuel consumption ratios, and vehicle kilometers travelled as reported by Environment Canada (2012). In the Ontario, model-ready CO inventory, emission sources are classified by SCC (Source Classification Code) and were mapped to NFR (Nomenclature for Reporting) codes for accurate cross-reference with the NIR CO_2 and CO estimates. Provincial totals for CO_2 and CO are estimated based on the NFR sources that are included in the sector, producing the following NIR sector-averaged CO_2:CO ratio:

228 $$CO_{2(sector,kt)} = CO_{(sector,kt)} * \frac{CO_{2(Ontario\ sector,kt)}}{CO_{(Ontario\ sector,kt)}} \qquad \text{(Eq. 1)}$$

229 This sector-averaged CO_2:CO ratio is used to convert the APEI-based model-ready gridded CO
230 emissions fields into CO_2 emissions fields at the same spatial and temporal resolution. Because the
231 spatial and temporal variability of the sources of CO_2 are similar to those of CO, the fine-resolution
232 gridded CO sectoral emissions fields for Ontario were primarily used as spatial and temporal
233 proxies for CO_2 emissions; the use of NIR-based CO_2:CO ratios helps to produce realistic emissions
234 estimates of CO_2 despite uncertainties in CO emissions estimates. A detailed outline of this
235 conversion is presented for each of the seven CO emissions sectors in the following subsections.
236 Unless otherwise noted, temporal allocation of emissions in each sector is based on estimates made
237 available by SMOKE.

238 *2.4.1 Area emissions*

239 Area emissions are mostly small stationary sources that represent diffuse emissions that are not
240 inventoried at the facility level. In the APEI CO inventory, the major emission sources in the Area
241 sector include emissions from public electricity and heat production (1A1a), residential and
242 commercial plants (1A4a and 1A4b), stationary agriculture/forestry/fishing (1A4c), iron and steel
243 production (2C1), and pulp and paper (2D1). The NIR estimates an Ontario total from these (and
244 other minor sources) of 2.3 x10^4 kt CO_2 and 219 kt CO, producing a CO_2:CO ratio of 107 kt CO_2/kt
245 CO. This ratio was applied to every Area sector grid cell belonging to Ontario in the domain to
246 convert sector CO emissions to CO_2 emissions.

247 *2.4.2 Point emissions*

248 Point emissions are stationary sources in which emissions exit through a stack or identified
249 exhaust. In the APEI CO inventory, the major emission sources in the Point sector include public
250 electricity and heat production (1A1a), stationary combustion in manufacturing industries and

construction (1A2f), chemical industry (2B5a), pulp and paper (2D1), iron and steel production (2C1) and other metal production (2C5). Unlike the Area sector, we found that applying a single CO_2:CO ratio to every facility did not produce realistic CO_2 emissions due to the negligible emissions of CO and therefore highly variable CO_2:CO ratios (because of a small denominator). Therefore, we used ECCC Facility Reported Data (Environment Canada, 2015) to identify the geocoded location and annual average CO_2:CO for 48 individual facilities in Ontario (Table S1) and applied the specific CO_2:CO ratios to the grid cells where the facilities were located. In addition, stack height of individual facilities were included in the emission model to optimize plume rise. All other point sources (minor facilities) were scaled by a sector average CO_2:CO ratio of 313 kt CO_2/kt CO, calculated from Ontario total CO_2 and CO point-source emissions from the NIR. Temporal allocation of emissions in the Point sector are based on facility level operating schedule data collected by ECCC.

2.4.3 On-road mobile emissions

On-road emissions include the emissions from any on-road vehicles (quantified by the Statistics Canada Canadian Vehicle Survey) (Environment Canada, 2013). In the APEI CO inventory, the major emission sources in the On-road sector includes gasoline and diesel-powered light- and heavy-duty vehicles (1A3b). The NIR estimates an Ontario total from these (and other minor on-road sources) of 4.4×10^4 kt CO_2 and 1.5×10^3 kt CO, producing a CO_2:CO ratio of 29 kt CO_2/kt CO. This ratio was applied to every On-road grid cell belonging to Ontario in the domain to convert sector CO emissions to CO_2. Temporal allocation of emissions in the On-road sector is estimated using data collected in the FEVER (Fast Evolution of Vehicle Emissions from Roadways) campaign in 2010 (Gordon et al., 2012a; Gordon et al., 2012b; Zhang et al., 2012). There are challenges associated with using a single CO_2:CO ratio for all on-road vehicles (both gasoline and diesel powered) as well as for all hours of the day (e.g., cold-start emissions from vehicles are different than running emissions).

Therefore, the CO_2 On-road emissions estimated in this study are an approximation of a more complex reality.

2.4.4 Off-road mobile emissions

Off-road emissions include the emissions from any off-road vehicles that do not travel on designated roadways, including aircraft, all off-road engines (such as chainsaws, lawn mowers, snow blowers, and snowmobiles), and locomotives. In the APEI CO inventory, the major emission sources in the Off-road sector include civil aviation (1A3a), railways (1A3c), and agriculture/forestry/fishing: off-road vehicles and other machinery (1A4c). Similar to the Point sector, we found that applying a single CO_2:CO ratio to every grid cell did not produce realistic CO_2 emissions for the two major airports in the GTA, Pearson International Airport (hereafter referred to as Pearson Airport) and Billy Bishop Toronto City Airport (hereafter referred to as Billy Bishop Airport). Therefore, we used air quality assessment reports compiled for each airport (RWDI AIR Inc., 2009; RWDI AIR Inc., 2013) to identify the geocoded location and facility-specific annual average CO_2:CO ratio. Sources of emissions from each airport include aircraft (landing and take-off cycles), auxiliary power units, ground support equipment, roadways, airside vehicles, parking lots, stationary sources and training fires; note that emissions from aircrafts in-transit between airports, which are injected in the free troposphere, have not been included in this inventory (Moran et al., 2015; RWDI AIR Inc., 2009). Based on these two reports, we applied a ratio of 175 kt CO_2/kt CO to the grid cell containing Pearson Airport and a ratio of 20 kt CO_2/kt CO to the grid cell containing Billy Bishop Airport. All other off-road sources belonging to Ontario grid cells were scaled by a sector average CO_2:CO ratio of 7 kt CO_2/kt CO, calculated from NIR-reported Ontario total CO_2 and CO emissions. Similar to On-road emissions, there are challenges associated with using a single CO_2:CO ratio for all vehicles (both gasoline and diesel powered) as well as for all hours of the day.

298 Therefore, the CO_2 Off-road emissions estimated in this study are an approximation for a very
299 complex sector.

300 *2.4.5 Marine emissions*

301 Commercial marine emissions include the emissions from any marine vessels travelling on the
302 Great Lakes (quantified by the Statistics Canada *Shipping in Canada*) (Environment Canada, 2013).
303 In the APEI CO inventory, the major emission source in the Marine sector is national navigation
304 (1A3d). The NIR estimates an Ontario total from this source of 729 CO_2 and 0.86 kt CO, producing a
305 CO_2:CO ratio of 844 kt CO_2/kt CO. This ratio was applied to every marine grid cell in the domain to
306 convert sector CO emissions to CO_2. Note that inclusion of this source sector was desirable because
307 two of the CO_2 measurement stations considered in this study (Turkey Point and Hanlan's Point)
308 are near-shore stations.

309 *2.4.6 Residential and commercial emissions*

310 Residential and commercial CO_2 emissions reflect on-site combustion of natural gas for electricity
311 and heating, a source that we found was not included in the APEI CO inventory because of the high
312 efficiency of the furnaces and resulting low CO emissions. To include the CO_2 emissions from these
313 on-site furnaces, we used the Statistics Canada 2012 Report on Energy Supply and Demand to
314 quantify the amount of natural gas consumed by residential and commercial buildings in Ontario,
315 7.9×10^3 gigalitres (Gl) and 4.9×10^3 Gl respectively (Statistics Canada, 2012a). The Canadian NIR
316 estimated 1879 g CO_2 m^{-3} natural gas as the CO_2 emission factor specific for the province of Ontario,
317 based on data from a chemical analysis of representative natural gas samples and an assumed fuel
318 combustion efficiency of 99.5 % (Environment Canada, 2012). Using this emission factor, CO_2
319 emissions from residential and commercial on-site furnaces in Ontario were estimated to be 1.5 x
320 10^7 tonnes and 9.2 x 10^6 tonnes, respectively. These two emission totals were spatially allocated

using a "capped-total dwelling" spatial surrogate developed by ECCC and temporally allocated using the SMOKE emissions processing system (Moran et al., 2015).

2.5 Biogenic fluxes

The net ecosystem exchange fluxes used in our simulations were provided by the land surface component of the ECMWF forecasting system, C-TESSEL (Bousetta et al., 2013). Fluxes are extracted at the highest available resolutions, 15 x 15 km and 3 hour for January and February 2016 and 9 x 9 km and 3 hour for March. These data are interpolated in space and time to be consistent with our model resolution. With our main priority being understanding anthropogenic emissions in the GTA, we chose to analyze a period where the biogenic CO_2 flux is minimized and therefore this paper focuses on three winter months in 2016, January to March inclusive.

3.0 Results and Discussion

3.1 The SOCE inventory

Figure 1 displays the PanAm domain total anthropogenic CO_2 emissions estimated by the SOCE inventory for the province of Ontario portion (~0.02^o x 0.02^o) and by the FFDAS v2 inventory (0.1^o x 0.1^o) (FFDAS, 2010) for the remainder of the domain. Regions of high emissions typically correspond to population centers, for example the GTA in Ontario, Montreal and Quebec City in Quebec, and Chicago, Boston and New York City (amongst others) in the USA. Emissions from highways and major roadways are only clear in the province of Ontario (at higher spatial resolution) but industrial and large scale area sources are evident across the entire domain.

The total CO_2 emissions can be separated into contributions from the seven sectors in the province of Ontario described in Section 2.4. Figure 2 shows the anthropogenic CO_2 contributions

from the Area sector, Residential and Commercial sector, Point sector, Marine sector, On-road sector and Off-road sector, focused on southern Ontario and the GTA. If we consider emissions from a domain including the area solely around the GTA (indicated by the black-box in Figure 2a), the total CO_2 emissions estimated by the SOCE inventory is 94.8 Mt CO_2 per year, Table 2. Figures 2a and b display the CO_2 emissions from the Area sector and from Residential and Commercial natural gas combustion in southern Ontario. These two sectors combined represent the largest source of CO_2 in the black-box area (41.6 Mt CO_2/year, contributing 43.9 % of the total). The majority of these emissions are concentrated in the GTA and surrounding urban areas as a result of a significant portion of the population (64 %) being reliant on natural gas for heat production (Statistics Canada, 2007; Statistics Canada, 2012a). Figure 2c represents emissions from the Point sector, contributing 24.4 Mt CO_2/year, 25.7 % of the total. The largest point source emitters are located on the western shore of Lake Ontario (Hamilton and surrounding areas) as this area is one of the most industrialized regions of the country with intensive metal production activities. Figures 2d, e and f display CO_2 emissions from various transportation sectors, Marine, On-road, and Off-road respectively, which together contribute more than 30 % of total CO_2 emissions in the area within the black box. While emissions from marine activity are minimal, those from On-road and Off-road sources are significant (25.0 % and 5.3 %, respectively), concentrating on the major highways connecting the various population centres of the GTA to the downtown core, as well as at Pearson Airport located within the city.

3.2 Comparison of the SOCE inventory with other inventories

The EDGAR v4.2 inventory estimates CO_2 emissions on an annual basis and by sector based on Selected Nomenclature for Air Pollution (SNAP) sub-sectors while FFDAS v2 provides hourly mean grid cell totals. Table 2 shows a comparison between the sectoral CO_2 estimates of the SOCE and EDGAR v4.2 inventories (SNAP sectors were grouped to correspond to SOCE sectors, Table S2) as

well as the domain total estimated by the FFDAS v2 inventory for the area surrounding the GTA (the black-box area outlined in Figure 2a). There is a significant discrepancy between the CO_2 emissions estimated by the SOCE and EDGAR v4.2, inventories both in the relative sectoral contributions as well as domain total (percent difference >35 %). The largest sectoral discrepancies are in the Point and the On-road sectors, where the EDGAR v4.2 inventory estimates a contribution 1.9 and 1.7 times larger than that of the SOCE inventory, respectively. Figure 3 shows a comparison of the spatial distribution of the CO_2 inventory predicted by a) FFDAS v2, b) EDGAR v4.2, and c) SOCE (aggregated to 0.1^o x 0.1^o to match the resolution of EDGAR v4.2 and FFDAS v2) for the GTA area. Figure 3 reveals that the largest differences between the SOCE inventory and the EDGAR v4.2 inventory is the CO_2 emissions in the GTA; EDGAR v4.2 predicts much higher emissions in the GTA (in some grid cells, differences are an order of magnitude), particularly in the downtown core relative to the SOCE inventory.

Although there is no sectoral breakdown in the FFDAS v2 inventory, the domain total around the GTA can be compared to that of the SOCE inventory, Table 2. Unlike the comparison with the EDGAR v4.2 inventory, there is a closer agreement between the FFDAS v2 inventory and the SOCE inventory (difference of ~10 %). The comparison plots in Figure 3 show a good agreement of the spatial variability of emissions in the GTA between the FFDAS v2 and SOCE inventories; however, the gradient between urban and rural areas is not as sharp in the SOCE inventory as it is in the FFDAS v2 inventory. Furthermore, emissions along the western shore of Lake Ontario (Hamilton and the surrounding areas) are predicted to be larger in the SOCE inventory relative to FFDAS v2. The FFDAS v2 inventory was interpolated to 0.02^o x 0.02^o using a mass conservative interpolation scheme to allow the production of a difference plot of the two inventories, SOCE minus FFDAS v2, shown in Figure S1. The difference plot reveals the largest divergence between the inventories occurs in the GTA and Ottawa, with the FFDAS v2 inventory estimating >1000 g CO_2/second (~30 kt CO_2/year) more than the SOCE inventory in some grid

cells. In addition to similar spatial variability, the FFDAS v2 and SOCE inventories also have similar temporal variability. Figure S2 shows the diurnal profile of estimated emissions from January-March for both the FFDAS v2 and SOCE inventories for the black-box area in the PanAm domain. Both inventories allocate the highest emissions between 08:00 and 18:00 and the lowest emission between 00:00 and 5:00, however the amplitude of the diurnal cycle is higher in SOCE, and emissions in the morning are as high as in the afternoon. FFDAS allocates a relatively larger proportion of the emissions to the 15:00 – 19:00 period.

3.3 Preliminary analyses using the SOCE, FFDAS v2 and EDGAR v4.2 inventories with FLEXPART

To investigate the impact of the different inventories on ambient mixing ratios, preliminary analyses were run with footprints generated for every third hour of the day (i.e., 00h, 03h, 06h, 09h, etc.) by the FLEXPART Lagrangian particle dispersion model (Stohl et al., 2005) driven by GEM meteorology for two sites, Downsview and TAO. Footprint areas were multiplied by the inventory estimates to arrive at mixing ratio enhancements and then compared against the measured CO_2 gradient between the Downsview and TAO stations for the year 2014. Gradients were used to capture the CO_2 mixing ratios in the downtown core of the city (since Downsview and TAO are situated just north and south of downtown Toronto, respectively). Observed gradients ranged from +20 to -10 ppm. Figure S3 displays the measured and modelled CO_2 gradients. These results show that when the EDGAR v4.2 inventory was used, simulated CO_2 gradients were consistently overestimated by ~10-60 ppm relative to observations. Conversely, when the SOCE inventory was used, a higher level of agreement was obtained between simulated mixing ratios and measurements; however, none of the model simulations were able to capture times when the gradient was negative ($CO_{2,TAO} > CO_{2,Downsview}$), an effect we believe to be due to the TAO inlet being ~60 m above ground level and surrounded by many high-rise buildings creating canyon flows and turbulence which are not properly accounted for in GEM at this resolution. These factors

416 contributed to the decommissioning of TAO in January 2016. The poor performance of our model
417 system when using the EDGAR v4.2 inventory to simulate CO_2 mixing ratios was also found by a
418 study quantifying on-road CO_2 emissions in Massachusetts, USA (Gately et al., 2013). In this study,
419 EDGAR emission estimates were found to be significantly larger than any other inventory by as
420 much as 9.3 million tons, or >33 %. The difference in estimates between the EDGAR v4.2 and the
421 SOCE inventories is likely explained by their underlying differences in methodology. Being a global
422 product and not specifically designed for mesoscale applications, the EDGAR v4.2 inventory
423 estimates CO_2 emissions based on country-specific activity data and emission factors, however the
424 spatial proxies used to disaggregate the data are not always optimal. A study performed by
425 McDonald et al. (2014) showed that the use of road density as a spatial proxy for vehicle emissions
426 in EDGAR v4.2 causes an overestimation of emissions in population centers (McDonald et al., 2014).
427 Given the much larger emission estimates for On-road CO_2 from EDGAR v4.2 (Table 2), this also
428 seems to be an issue in the GTA. Based on this large discrepancy, the EDGAR v4.2 inventory was not
429 further used in this study and we focussed on the inventories developed for regional scale studies.

430 When similar preliminary analyses were run with FLEXPART footprints using the FFDAS v2
431 inventory, Figure S3, good agreement was observed with CO_2 gradients measured between the
432 Downsview and TAO stations. We are confident that the enhanced measurement agreement
433 between the FFDAS v2 and SOCE relative to EDGAR v4.2 is due to improved methodology; spatial
434 allocation of emissions in FFDAS v2 is achieved through the use of satellite observations of
435 nightlights from human settlements from the U.S. Defense Meteorological Satellite Program
436 Operational Linescan System (DMSP-OLS).

437 Beyond the differences in methodology for estimating and allocating emissions, it is
438 important to note that the emissions reported in Table 2 by the FFDAS v2, SOCE and EDGAR v4.2
439 inventories also fundamentally differ in time period quantified. The emissions reported for both

FFDAS v2 and the SOCE are based on emissions from three winter months (January-March 2010) extrapolated for the entire year. However, emissions from EDGAR v4.2 are annual averages of all twelve months of 2010. Since CO_2 emissions in the GTA are higher in the winter months relative to the summer months because of increased building and home heating, it is likely that the average annual estimates of SOCE and FFDAS v2 are slightly overestimated. This does not affect the relative agreement between SOCE and FFDAS v2 however it does further increase the divergence between the EDGAR v4.2 and SOCE and FFDAS v2 inventories. Following this and the improved agreement with observations, the FFDAS v2 inventory was used with the SOCE inventory for all subsequent modelling analyses.

3.4 Simulation of CO_2 mixing ratios in the Greater Toronto Area

We used the GEM-MACH chemistry-transport model and the SOCE and FFDAS v2 inventories to simulate hourly CO_2 mixing ratios in the PanAm domain. The model framework was evaluated for a continuous three-month period, January-March 2016 using four sampling locations in the GTA, Figure 1 (note that measurements for the Hanlan's Point site were not available until January 14, 2016). Figure 4 displays afternoon (12:00-16:00 EST) measured and simulated CO_2 mixing ratios produced with the SOCE and FFDAS v2 inventories for the two emissions scenarios described in Section 2.3 for the month of February (Figures S4 and S5 show the same figure for other months). We chose to present only afternoon data as this is the time of day when the mixed layer is likely to be the most well-developed; nighttime and morning data showed largest variations in observations as a result of the shallow boundary layer causing surface emissions to accumulate within the lowest atmospheric layers (Breon et al., 2015; Chan et al., 2008; Gerbig et al., 2008). During the night, atmospheric mixing ratios are most sensitive to vertical mixing, an atmospheric process that is difficult to model for stable boundary layers.

463 The time series comparisons at all four sites demonstrate the model's general ability to
464 capture variability in observations of CO_2, albeit with better skill for the Downsview and Egbert
465 sites (this is particularly clear when we look at model-measurement difference plots, Figure S6).
466 The model is able to capture many extreme events of mixing ratio increases and decreases, such as
467 February 11-14, 2016 at the Downsview site; however, some short time periods are poorly
468 simulated, such as January 21-23, 2016 at Hanlan's Point, when the model significantly
469 overestimated measured CO_2. Generally, mixing ratios simulated by the FFDAS v2 inventory are
470 similar or larger than those produced when the SOCE inventory is used, with differences most
471 noticeable at the Downsview and Hanlan's Point sites. This was expected as the difference plot
472 shown in Figure S1 reveals that the SOCE and FFDAS v2 inventories diverge the most in the GTA
473 (where the Downsview and Hanlan's Point sites are located) and are more similar in rural areas
474 (where the Turkey Point and Egbert sites are located).

475 Measured CO_2 mixing ratios have a typical diurnal pattern, in which mixing ratios are higher
476 at night and lower during the day, despite higher emissions during the day. This results from the
477 daily cycle of the mixed layer, which is shallow at night due to thermal stratification and deepens
478 during the day due to solar heating of the surface. Figure 5 displays the measured and modelled
479 mean diurnal profile of CO_2 at the four sites in our network using data from January-March, 2016
480 (note difference in y-axis scale for urban vs. rural sites). At all four sites, the shapes of the modelled
481 and measured mixing ratios throughout the day agree very well, suggesting that the GEM
482 meteorology in our framework is capturing the diurnal variation in emissions and the boundary
483 layer evolution. At the Downsview site, there is a very strong agreement between the modelled and
484 measured diurnal profiles when using the SOCE inventory, whereas the FFDAS v2 simulated profile
485 largely overestimates mixing ratios, particularly at nighttime. This is consistent with the FFDAS
486 inventory having larger emissions than the SOCE inventory during the night (Fig S2). At the
487 Hanlan's Point site, a difference of $\sim$ 5 ppm CO_2 is observed when using the SOCE inventory relative

to measurements; however, similar to the Downsview site, the FFDAS v2 simulated profile has a larger difference of ~10 ppm CO_2. At both the Egbert and Turkey Point sites, the use of both inventories similarly overestimates the diurnal pattern of CO_2 mixing ratios by ~3-5 ppm, again likely a result of the similarities of these two inventories at these sites, Figure S1. At all four sites, it is possible that some of the biases that are observed in simulated CO_2 mixing ratios may arise from inaccuracies in the boundary CO_2 provided by MACC; this aspect was not, however, further explored in this study.

3.5 Quantifying model-measurement agreement

Figure 6 shows scatter plots of afternoon (12:00-16:00 EST) modelled versus measured CO_2 mixing ratios from January- March, 2016 at the four sites used in this study. The top row shows the correlation between measured and modelled mixing ratios using the SOCE inventory and the bottom row shows the correlation using the FFDAS v2 inventory. It is immediately clear that there is a stronger model-measurement correlation at the Downsview and Egbert sites ($R > 0.75$) relative to that of Hanlan's Point or Turkey Point ($R < 0.53$). The difficulty with accurately simulating CO_2 mixing ratios at Hanlan's Point and Turkey Point may arise from their proximity to shorelines, Hanlan's Point to Lake Ontario and Turkey Point to Lake Erie (see Figure 1). Differential heating of land versus water near these lakes creates pressure gradients driving unique circulation patterns (Burrows, 1991; Sills et al., 2011). These circulation patterns are difficult for models to capture and therefore may contribute to the relatively poor correlation observed at Hanlan's Point and Turkey Point.

It is also clear from Figure 6 that simulating CO_2 mixing ratios at the Egbert and Turkey Point sites using either the FFDAS v2 or the SOCE inventory results in similar performance, likely because the emissions estimated by the two inventories are similar in the vicinity of these two rural sites (see also Figure 5). However at both the Downsview and Hanlan's Point sites, using the SOCE

512 inventory provided a slightly higher correlation and reduced RMSE and MB relative to using the
513 FFDAS v2 inventory. The improvement by using the SOCE inventory is likely a result of both the
514 improved spatial resolution (2.5 km versus 10 km), and therefore more accurate allocation of
515 emissions to grid cells, and also a better estimation of emission magnitudes, as large differences are
516 shown in Figures 3 and S1.

517 *3.6 Sectoral contributions to simulated CO_2 mixing ratios*

518 One of the major advantages of the SOCE inventory over the FFDAS v2 inventory is the availability
519 of sectoral emission estimates. Figure 7 displays the sectoral percent contributions to diurnal CO_2
520 mixing ratio enhancements (calculated as local CO_2 mixing ratios above the MACC estimated
521 background) for the Downsview station in February 2016 averaged by the day of week (Figures S7
522 and S8 displays the same for other months). This figure clearly demonstrates the importance of
523 Area emissions (defined here as the sum of the Area + Residential natural gas combustion +
524 Commercial natural gas combustion) to simulated CO_2 mixing ratios, reaching ~80 % contribution
525 in the early morning and late evening, consistent with times when emissions from home heating are
526 the dominant source of CO_2. Contributions from Area emissions decrease to ~35 % midday, which
527 coincides with when emissions from other sources, such as On-road, gain importance. In the
528 midday, emissions from the On-road sector can contribute ~50 %, which is consistent with
529 transportation patterns of the times when the population is travelling to and from work and other
530 activities. The relative contributions to CO_2 mixing ratios from point source emissions is quite
531 variable during the course of a day and week, but generally seems to increase in the early morning
532 and evening and can contribute a significant portion of total CO_2 emissions (up to ~20 %). Figure 7
533 indicates that biogenic sources of CO_2 play a negligible role during January-March in the GTA (the
534 Biogenic line is not visible because it is located on the zero line underneath the Marine line). Recent
535 studies, however, have shown the importance of the biospheric contribution (up to ~132-308 g CO_2

536 km^{-2} s^{-1}) to measured CO_2 in urban environments during the growing season (Decina et al., 2016).
537 Therefore, this finding supports the importance of modelling CO_2 in the wintertime in cities like the
538 GTA to avoid complications associated with biospheric contributions. The new ability to
539 understand the sectoral contributions to CO_2 mixing ratios in the GTA and southern Ontario has
540 implications from a policy perspective; with recent initiatives to curb CO_2 emissions, understanding
541 from which sector the CO_2 is being emitted could be useful to assess how effective applied
542 mitigation efforts have been or where to target future efforts. These efforts could be complemented
543 by running simulations with additional tracers, such as carbon monoxide (CO), nitrogen oxides
544 (NO_x), or stable carbon isotopes (^{12}C and ^{13}C) to gain further insight.

545 *4.0 Conclusions*

546 We presented the SOCE inventory for southern Ontario and the GTA, the first, to our knowledge,
547 high-resolution CO_2 inventory for southern Ontario and for a Canadian metropolitan region. The
548 SOCE inventory provides CO_2 emissions estimates at 2.5 km x 2.5 km spatial and hourly temporal
549 resolution for seven sectors: Area, Residential natural gas combustion, Commercial natural gas
550 combustion, Point, Marine, On-road and Off-road. When compared against two existing CO_2
551 inventories available for southern Ontario, the EDGAR v4.2 and the FFDAS v2 inventories, using
552 FLEXPART footprints, the SOCE inventory had improved model-measurement agreement; FFDAS
553 v2 agreed well with in situ measurements, but the EDGAR v4.2 inventory systematically
554 overestimated mixing ratios. We developed a model framework using the GEM-MACH chemistry-
555 transport model on a high-resolution 2.5 km x 2.5 km grid coupled to the SOCE and FFDAS v2
556 inventories for anthropogenic CO_2 emissions and C-TESSEL for biogenic CO_2 fluxes. We compared
557 output simulations to observations made at four stations across southern Ontario and for three
558 winter months, January – March, 2016. Model-measurement agreement was strong in the afternoon
559 using both anthropogenic inventories, particularly at the Downsview and Egbert sites. Difficulty in

capturing mixing ratios at the Hanlan's Point and Turkey Point sites was hypothesized to be a result of their close proximity to shorelines (Lake Ontario and Lake Erie, respectively) and the model's inability to capture the unique circulation patterns that occur in those environments. Generally, across all stations and months, simulations using the SOCE inventory resulted in higher model-measurement agreement than those using the FFDAS v2 inventory, quantified using R, RMSE and mean bias. In addition to improved agreement, the primary advantage of the SOCE inventory over the FFDAS v2 inventory is the sectoral breakdown of emissions; using average day of week diurnal mixing ratio enhancements, we were able to demonstrate that emissions from area sources can contribute >80 % of CO_2 mixing ratio enhancements in the early morning and evening with on-road sources contributing >50 % midday. The applications of the SOCE inventory will likely show future utility in understanding the impacts of CO_2 reduction efforts in southern Ontario and identify target areas requiring further improvement.

Author Contributions

The SOCE inventory was prepared by Stephanie C. Pugliese, with critical input from Felix Vogel and Jennifer Murphy. The CO inventory which the SOCE inventory is based upon and the CO_2 emissions fields for residential and commercial natural-gas combustion were provided by Michael D. Moran, Junhua Zhang and Qiong Zheng. The GEM-MACH modelling analyses were performed by Shuzhan Ren and Craig Stroud. The ambient CO_2 data were collected by Douglas Worthy and his team at Environment and Climate Change Canada. The MACC and C-TESSEL products used in our model simulations were provided by Gregoire Broquet. The data was analyzed and interpreted for publication by Stephanie C. Pugliese. This manuscript was written by Stephanie C. Pugliese, with critical input from Jennifer Murphy, Felix Vogel and Mike Moran.

Acknowledgements

The authors are thankful to Robert Kessler, Michelle Ernst, Lauriant Giroux, Senen Racki and Lin Huang for their efforts collecting the $^{12}CO_2$ and $^{13}CO_2$ measurements at Environment and Climate Change Canada. They would also like to thank Elton Chan for providing the FLEXPART footprints and for Pegah Baratzadeh for her help creating the SOCE inventory.

591 *References*

592 Bousetta, S., Balsamo, G., Beljaars, A., Panareda, A. A., Calvet, J. C., Jacobs, C., van den Hurk, B.,
593 Viterbo, P., Lafont, S., Dutra, E., Jarlan, L., Balzarolo, M., Papale, D., and van der Werf, G. (2013).
594 Natural Land Carbon Dioxide Exchanges in the ECMWF Integrated Forecasting System:
595 Implementation and Offline Validation. *Journal of Geophysical Research: Atmospheres, 118*,
596 5923-5946.

597 Breon, F. M., Broquet, G., Puygrenier, V., Chevallier, F., Xueref-Remy, I., Ramonet, M., Dieudonne, E.,
598 Lopez, M., Schmidt, M., Perrussel, O., and Cias, P. (2015). An Attempt at Estimating Paris Area
599 CO_2 Emissions from Atmospheric Concentration Measurements. *Atmospheric Chemistry and*
600 *Physics, 15*(1707), 1724.

601 Burrows, W. R. (1991). Objective Guidance for 0–24-Hour and 24–48-Hour Mesoscale Forecasts of
602 Lake-Effect Snow using CART. *American Meteorological Society, 6*, 357-378.

603 C40 Cities. (2016). C40 Cities: Global Leadership on Climate Change. Retrieved 10/12, 2016, from
604 http://www.c40.org/cities/toronto

605 Chan, D., Ishizawa, M., Higuchi, K., Maksyutov, S., and Chen, J. (2008). Seasonal CO_2 Rectifier Effect
606 and Large-Scale Extratropical Atmospheric Transport. *Journal of Geophysical Research,*
607 *113*(D17309) doi:doi:10.1029/2007JD009443

608 Côté, J., Desmarais, J. -G., Gravel, S., Méthot, A., Patoine, A., Roch, M., and and Staniforth, A. (1998b).
609 The Operational CMC/MRB Global Environment Multiscale (GEM) Model. Part II: Results.
610 *Monthly Weather Review, 126*, 1397-1418.

611 Côté, J., Gravel, S., Méthot, A., Patoine, A., Roch, M., and and Staniforth, A. (1998a). The Operational
612 CMC/MRB Global Environmental Multiscale (GEM) Model. Part 1: Design Considerations and
613 Formulation. *Monthly Weather Review, 126*, 1373-1395.

614 Decina, S. M., Hutyra, L. R., Gately, C. K., Getson, J. M., Reinmann, A. B., Short Gianotti, A. G., and
615 Templer, P. H. (2016). Soil Respiration Contributes Substantially to Urban Carbon Fluxes in the
616 Greater Boston Area. *Environmental Pollution, 212*, 433-439.

617 EDGAR. (2010). Emission Database for Global Atmospheric Research Release Version 4.2 of the
618 European Commission. Joint Research Centre (JRC)/Netherlands Environmental
619 Assessment Agency (PBL). Retrieved 06/29, 2016, from http://edgar.jrc.ec.europa.eu

620 Environment Canada. (2011). Canadian Greenhouse Gas Measurement Program. Retrieved 10/07,
621 2016, from https://www.ec.gc.ca/mges-ghgm/

622 Environment Canada. (2012). National Inventory Report 1990-2010: Greenhouse Gas Sources and
623 Sinks in Canada. Retrieved 10/07, 2016, from http://www.ec.gc.ca/ges-ghg/

624 Environment Canada. (2013). Manual for the Compilation of Canada's 2010 Air Pollutant Emissions.
625 Catalogue no. En14-87/2013E-PDF. Retrieved 10/07, 2016, from
626 http://www.ec.gc.ca/Publications/default.asp?lang=En&xml=8A08B403-C85E-4612-A958-
627 3F24446A61DB

628 Environment Canada. (2015). Reported Facility Greenhouse Gas Data. Retrieved 10/07, 2016, from
629 http://www.ec.gc.ca/ges-ghg/donnees-data/index.cfm?lang=En

630 FFDAS. (2010). Fossil Fuel Data Assimilation System (FFDAS). Retrieved 06/29, 2016, from
631 http://hpcg.purdue.edu/FFDAS/

Framework for Public Review and Engagement. (2007). Change is in the Air: Toronto's Commitment to an Environmentally Sustainable Future. Retrieved 10/12, 2016, from www.toronto.ca/legdocs/mmis/2007/ex/bgrd/backgroundfile-2428.pdf

Gately, C. K., Hutyra, L. R., Sue Wing, I., and Brondfield, M. N. (2013). A Bottom-Up Approach to on-Road CO_2 Emissions Estimates: Improved Spatial Accuracy and Applications for Regional Planning. *Environmental Science and Technology, 47*, 2423-2430.

Gerbig, C., Korner, S., and Lin, J. C. (2008). Vertical Mixing in Atmospheric Tracer Transport Models: Error Characterization and Propagation. *Atmospheric Chemistry and Physics, 8*, 591-602.

Gong, W., Makar, P. A., Zhang, J., Milbrandt, J., Gravel, S., Hayden, K. L., Macdonald, A. M., and Leaitch, W. R. (2015). Modelling Aerosol-Cloud-Meteorology Interaction: A Case Study with a Fully Coupled Air Quality Model (GEM-MACH). *Atmospheric Environment, 115*, 695-715.

Gordon, M., Staebler, R. M., Liggio, J., Li, S., Wentzell, J., Lu, G., Lee, P., and Brook, J. R. (2012a). Measured and Modeled Variation in Pollutant Concentration Near Roadways. *Atmopsheric Environment, 57*, 138-145.

Gordon, M., Staebler, R. M., Liggio, J., Makar, P., Li, S., Wentzell, J., Lu, G., Lee, P., and Brook, J. R. (2012b). Measurements of Enhanced Turbulent Mixing Near Highways. *Journal of Applied Meteorology and Climatology, 51*, 1618-1632.

Gurney, K. R., Mendoza, D. L., Zhou, Y., Fischer, M. L., Miller, C. C., Geethakumar, S., and De La Rue du Can, S. (2009). High Resolution Fossil Fuel Combustion CO_2 Emission Fluxes for the United States. *Environmental Science and Technology, 43*, 5535-5541.

652 Gurney, K. R., Razlivanvov, I., Song, Y., Zhou, Y., Benes, B., and Abdul-Massih, M. (2012).
653 Quantification of Fossil Fuel CO_2 Emissions on the Building/Street Scale for a Large U.S. City.
654 *Environmental Science and Technology, 46*(21), 12194-12202.

655 IPCC-WG3. (2014). Climate Change 2014: Mitigation of Climate Change.Working Group III
656 Contribution to the Fifth Assessment Report of the Intergovernmental Panel on Climate
657 Change. Retrieved 10/12, 2016, from http://www.ipcc.ch/report/ar5/wg3/

658 McDonald, B. C., McBride, Z. C., Martin, E. W., and Harley, R. A. (2014). High-Resolution Mapping of
659 Motor Vehicle Carbon Dioxide Emissions. *Journal of Geophysical Research: Atmospheres, 119*,
660 5283-5298.

661 Miller, S. M., and Michalak, A. M. (2016). Constraining Sector-Specific CO_2 and CH_4 Emissions in the
662 United States. *Atmospheric Chemistry and Physics Dicsussions,* doi:doi:10.5194/acp-2016-643

663 Moran, M., Zheng, Q., Zhang, J. and Pavlovic, R. (2015). RAQDPS Version 013: Upgrades to the CMC
664 Operational Regional Air Quality Deterministic Prediction System Released in June 2015.
665 Retrieved 10/07, 2016, from
666 http://collaboration.cmc.ec.gc.ca/cmc/cmoi/product_guide/docs/lib/op_systems/doc_opchan
667 ges/Technical_Note_GEM-MACH10_v1.5.3+SET2.1.1_Emissions_9Nov2015.pdf

668 Moran, M. D., Dastoor, A., & Morneau, G. (2013). Long-range transport of air pollutants and regional
669 and global AQ modelling. In E. Taylor, & A. McMillan (Eds.), *Air Quality Management - Canadian*
670 *Perspectives on a Global Issue* (pp. 69-98) Springer.

671 Ontario. (2016). Ontario's Five Year Climate Change Action Plan 2016-2020. Retrieved 09/14, 2016,
672 from https://www.ontario.ca/page/climate-change-action-plan

673 Patarasuk, R., Gurkey, K. R., O'Keeffe, D., Song, Y., Huang, J., Rao, P., Buchert, M., Lin, J. C., Mendoza,
674 D., and Ehleringer, J. R. (2016). Urban High-Resolution Fossil Fuel CO_2 Emissions Quantification
675 and Exploration of Emission Drivers for Potential Policy Applications. *Urban Ecosytems, 19*(3),
676 1013-1039.

677 Pavlovic, R., Chen, J., Anderson, K., Moran, M. D., Beaulieu, P., Davignon, D., and Cousineau, S. (2016).
678 The FireWork Air Quality Forecast System with Near-Real-Time Biomass Burning Emissions:
679 Recent Developments and Evaluation of Performance for the 2015 North American Wildfire
680 Season. *Journal of the Air and Waste Management Association, 66*(9), 819-841.

681 Pillai, D., Gerbig, C., Ahmadov, R., Rodenbeck, C., Kretschmer, R., Koch, T., Thompson, R., Neininger,
682 B., and Lavrie, J. V. (2011). High Resolution Simulations of Atmospheric CO_2 Over Complex
683 Terrain - Representing the Ochsenkopf Mountain Tall Tower. *Atmospheric Chemistry and*
684 *Physics, 11*, 7445-7464.

685 PIRD. (2016). Air Pollutant Emission Inventory Report (APEIR) 1990-2014. Retrieved 10/07, 2016,
686 from http://www.ec.gc.ca/Air/89ED82E9-CA92-424E-9FD1-
687 C57235A04CE0/Air%20Pollutant%20Emission%20Inventory%20Report%201990-2014.pdf

688 RWDI AIR Inc. (2009). *2007 Emissions Inventory Toronto Pearson International Airport, Toronto,*
689 *Ontario.* Retrieved 10/07, 2016, from
690 https://www.torontopearson.com/uploadedFiles/Pearson/Content/About_Pearson/Environ
691 ment/090430_TPIA_Emissions_Inventory_Final_Report.pdf

692 RWDI AIR Inc. (2013). *Billy Bishop Toronto City Airport (BBTCA) Final Report: Air Quality Review.*
693 Retrieved on 10/07, 2016 from

https://www1.toronto.ca/City%20Of%20Toronto/Waterfront%20Secretariat/Shared%20Content/Files/BBTCA/131115%20BBTCA%20Final%20Report%201400311.pdf

Sills, D., Brook, J., Levy, I., Makar, P., Zhang, J., and Taylor, P. (2011). Lake Breezes in the Southern Great Lakes Region and their Influence during BAQS-Met 2007. *Atmospheric Chemistry and Physics, 11*, 7955-7973.

Statistics Canada. (2007). Households and the Environment: Energy Use. Retrieved 12/04, 2012, from http://www.statcan.gc.ca/pub/11-526-s/2010001/t002-eng.pdf

Statistics Canada. (2009). Table 3.4: Total and Urban Land Area, 1996, 2001 (Modified) and 2006. Retrieved 10/12, 2016, from http://www.statcan.gc.ca/pub/92f0138m/2008001/t/4054949-eng.htm

Statistics Canada. (2011). Population, Urban and Rural, by Province and Territory (Canada). Retrieved 10/12, 2016, from http://www.statcan.gc.ca/tables-tableaux/sum-som/l01/cst01/demo62a-eng.htm

Statistics Canada. (2012a). Report on Energy Supply and Demand. Retrieved 12/04, 2015, from http://www.statcan.gc.ca/pub/57-003-x/2015001/t037-eng.pdf

Statistics Canada. (2012b). *Focus on Geography Series, 2011 Census.* Statistics Canada Catalogue no. 98-310-XWE2011004. Retrieved 08/13, 2013, from https://www12.statcan.gc.ca/census-recensement/2011/as-sa/fogs-spg/Facts-cma-eng.cfm?LANG=Eng&GK=CMA&GC=535

Stohl, A,. Forster, C., Frank, A., Seibert, P., & Wotawa, G. (2005). Technical note: The Lagrangian particle dispersion model FLEXPART version 6.2. *Atmospheric Chemistry and Physics, 5*, 2461-2474.

715 Talbot, D., Moran, M. D., Bouchet, V., Creview, L. -P., Menard, S., Kallur, A., & and the GEM-MACH
716 Team. (2008). Development of a new canadian operational air quality forecast model. In C.
717 Borrego, & A. I. Miranda (Eds.), *Air Pollution Modeling and its Application XIX* (pp. 470-478)
718 Springer Science and Business Media.

719 Wang, R., Tao, S., Ciais, P., Shen, H. Z., Huang, Y., Chen, H., Shen, G. F., Wang, B., Li, W., Zhang, Y. Y., Lu,
720 Y., Zhu, D., Chen, Y. C., Liu, X. P., Wang, W. T., Wang, X. L., Liu, W. X., Li, B. G., and and Piao, S. L.
721 (2013). High-Resolution Mapping of Combustion Processes and Implications for CO_2
722 Emissions. *Atmospheric Chemistry and Physics, 13*, 5189-5203.

723 WHO. (2015). Global Health Observatory (GHO) Data: Urban Population Growth. Retrieved 2/3,
724 2015, from
725 http://www.who.int/gho/urban_health/situation_trends/urban_population_growth_text/en/

726 Worthy, D. E., Platt, A., Kessler, R., Ernst, M., Audette, C., & Racki, S. (2005). *An update on the*
727 *canadian GHG measurement program, in: Report of the 12th WMO/IAEA meeting of experts on*
728 *carbon dioxide concentration related tracer measurement techniques.* (No. 162). Toronto,
729 Canada: World Meteorological Organization Atmosphere Watch.

730 Zhang, J., Zheng, Q., Moran, M. D., Gordon, M., Liggio, J., Pakar, P., Stroud, C. & Taylor, B. (2012).
731 *Improvements to SMOKE processing of canadian on-road mobile emissions.* 20th Emissions
732 Inventory Conference, 13-16 Aug., Tampa, 13pp. [see
733 http://www.epa.gov/ttn/chief/conference/ei20/session1/jzhang.pdf]

734 Zhao, Y., Nielsen, C. P., and McElroy, M. B. (2012). China's CO_2 Emissions Estimated from the Bottom
735 Up: Recent Trends, Spatial Distributions and Quantification of Uncertainties. *Atmospheric*
736 *Environment, 59*, 214-223.

Table 1: **Summary of atmospheric measurement programs in Southern Canada operated by Environment and Climate Change Canada**

Start Date	Site Name	Coordinates	Elevation (asl)	Intake Height	In-situ Instrumentation
March, 2005	Egbert	44.231037N, 79.783834W	251m	3m, 25m*	NDIR
November, 2010	Downsview	43.780491N, 79.468010W	198m	20m	NDIR
November, 2012	Turkey Point	42.635368N, 80.557659W	231m	35m	CRDS
June, 2014	Hanlan's Point	43.612201N 79.388705W	87m	10m	CRDS

* At Egbert, a 25 m tower was installed in March 9, 2009

NDIR = Non-dispersive infrared

CRDS = cavity ring-down spectroscopy

743 **Table 2: Anthropogenic CO_2 emissions for the year 2010 in the black-box area (shown in**
744 **Figure 2a) by sector. Values in parentheses indicate the percentage contribution of the**
745 **sector to the total CO_2 emissions in the black-box area.**

Sector	FFDAS v2‡ CO_2 Inventory (Mt CO_2/year)	EDGAR v4.2# CO_2 Inventory (Mt CO_2/year)	SOCE CO_2 Inventory (Mt CO_2/year)
Area*	-	46 (33.9 %)	42 (43.9 %)
Point	-	46 (33.7 %)	24 (25.7 %)
Marine	-	0.1 (0.10 %)	0.1 (0.10 %)
On-road	-	41 (30.2 %)	24 (25.0 %)
Off-road	-	3 (2.2 %)	5 (5.3 %)
Total	105	136	95

746 *Area sector represents the summation of Area + Residential + Commercial natural gas combustion.
747 #The EDGAR inventory v4.2 can be found at http://edgar.jrc.ec.europa.eu.
748 ‡The FFDAS v2 inventory can be found at http://hpcg.purdue.edu/FFDAS/.
749

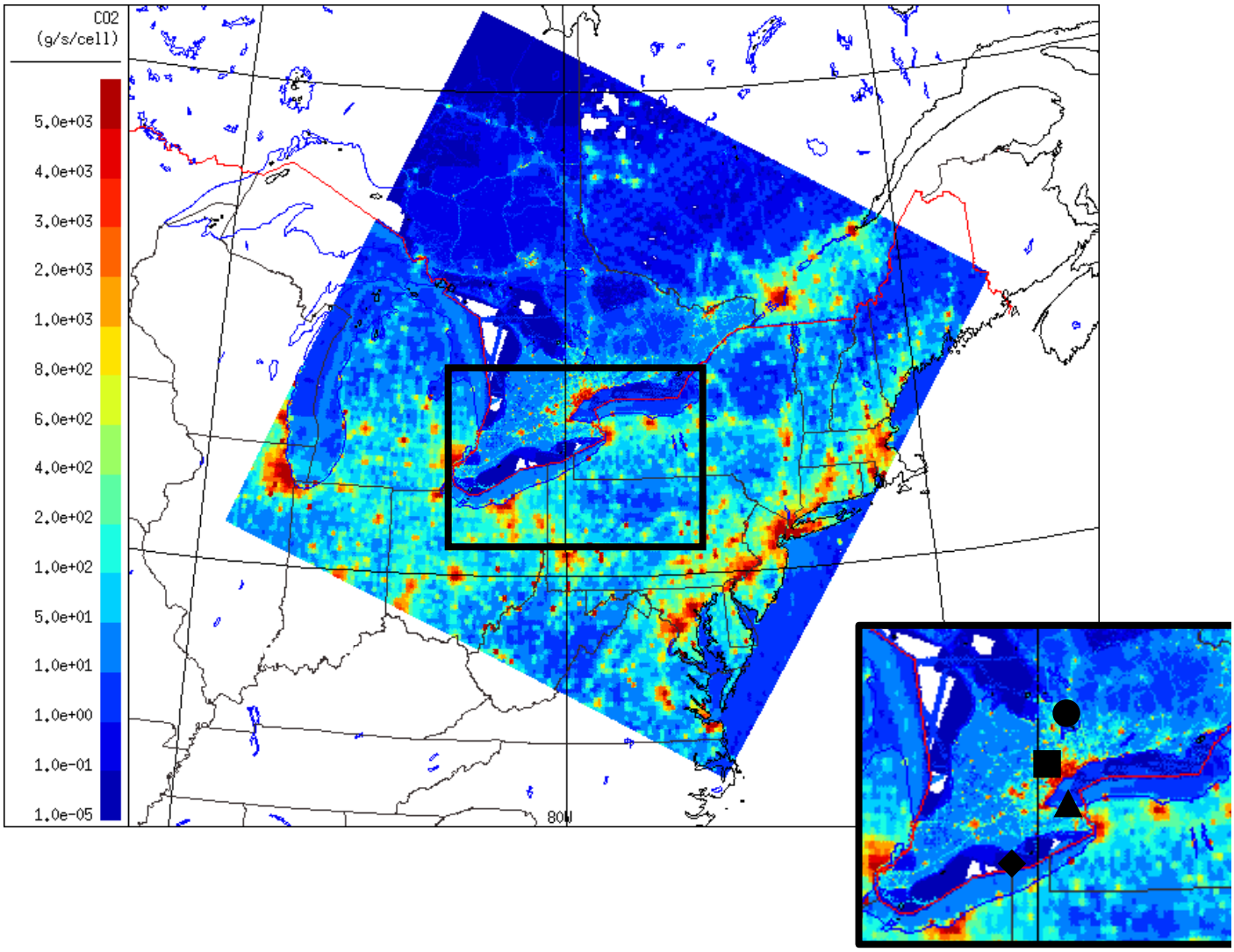

Figure 1: Total anthropogenic CO_2 emissions for a weekday in February 2010 estimated by the SOCE inventory for the province of Ontario and by the FFDAS v2 inventory for the remainder of the GEM-MACH PanAm domain. Locations of in-situ measurements of CO_2 in the Southern Ontario GHG Network are shown in the inset (Downsview = square, Egbert = circle, Hanlan's Point = triangle, Turkey Point = diamond). The Downsview and Hanlan's Point sites are both located in the GTA. Units: g CO_2/second/grid cell.

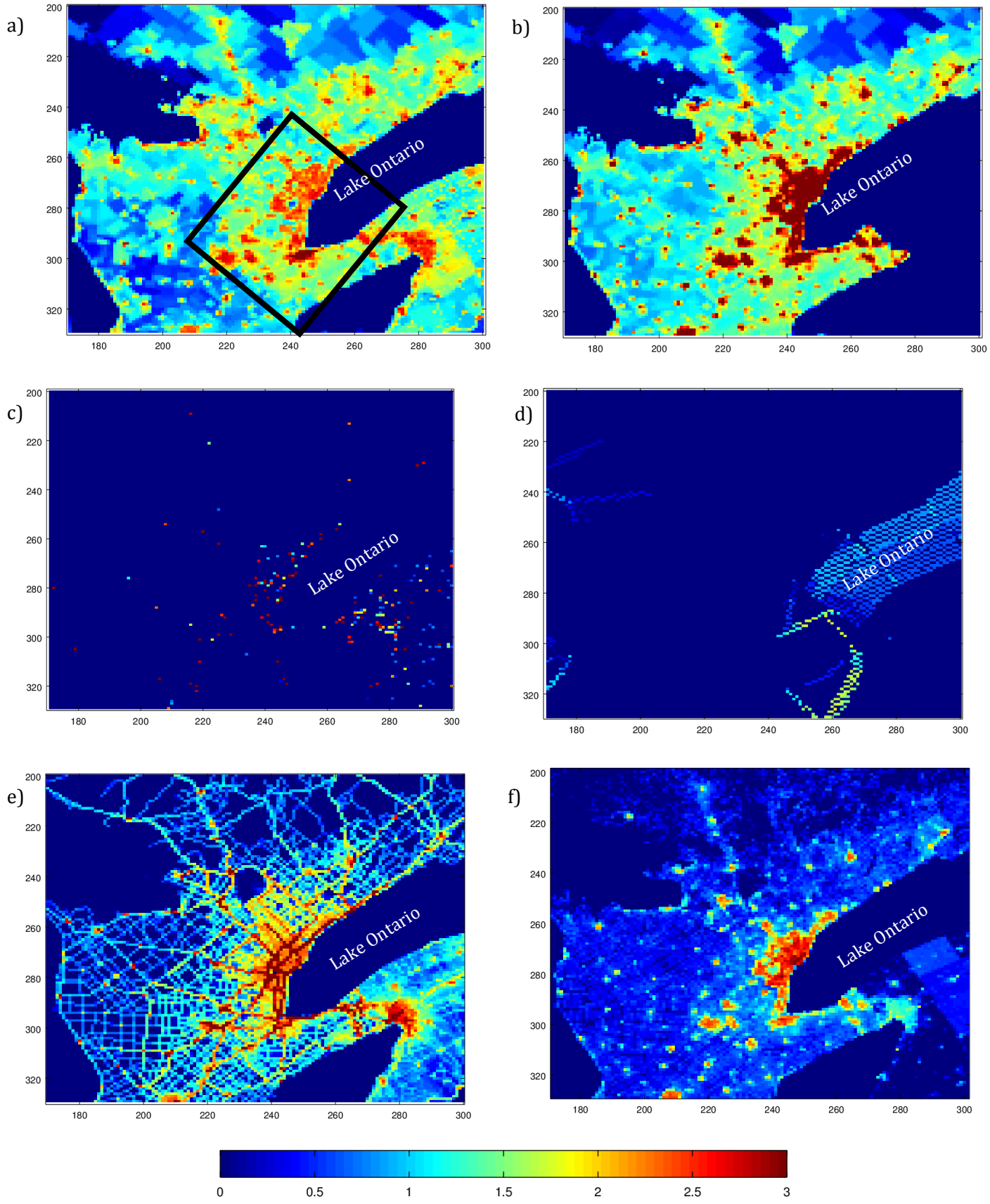
a)
b)
c)
d)
e)
f)
Lake Ontario
200
220
240
260
280
300
320
180
200
220
240
260
280
300
0
0.5
1
1.5
2
2.5
3

Figure 2: Anthropogenic CO_2 emissions for a weekday in February 2010 in southern Ontario. Emissions are estimated by the SOCE inventory for the (a) Area sector; (b) sum of the Residential and Commercial sectors; (c) Point sector; (d) Marine sector; (e) On-road sector; (f) Off-road sector. Units: $\log_{10}$(g CO_2/second/grid cell).

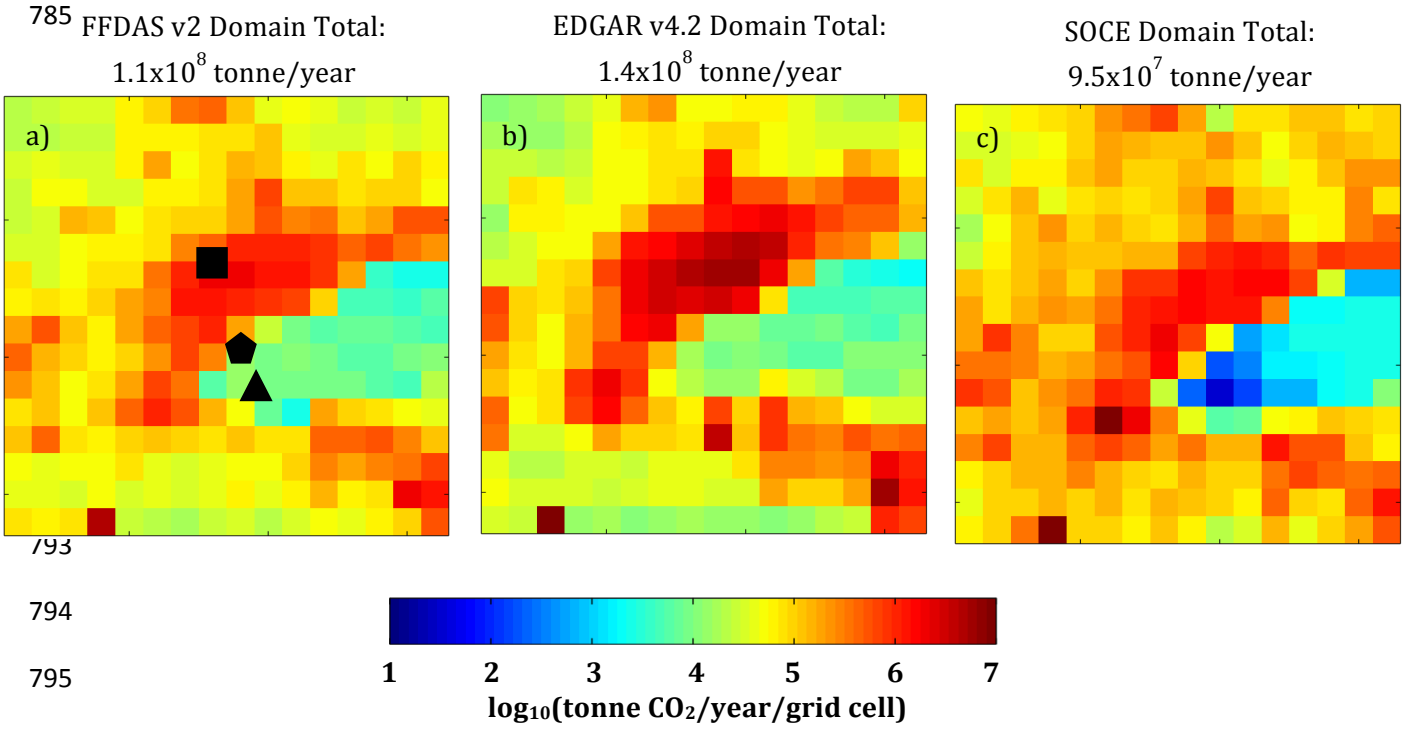

Figure 3: Comparison of spatial distribution of annual CO_2 emissions inventories for the black-box area (shown in Figure 2a) at 0.1° x 0.1° resolution. Panel a) shows the FFDAS v2 inventory estimate, Panel b) shows the EDGAR v4.2 inventory estimate and Panel c) shows the SOCE inventory estimate. Domain totals are shown on top of each panel and locations of in-situ measurements of CO_2 for three stations in the Southern Ontario GHG Network are shown on Panel a (Downsview = square, Hanlan's Point = triangle, TAO = pentagon). The other two stations, Egbert and Turkey Point, are located outside this area.

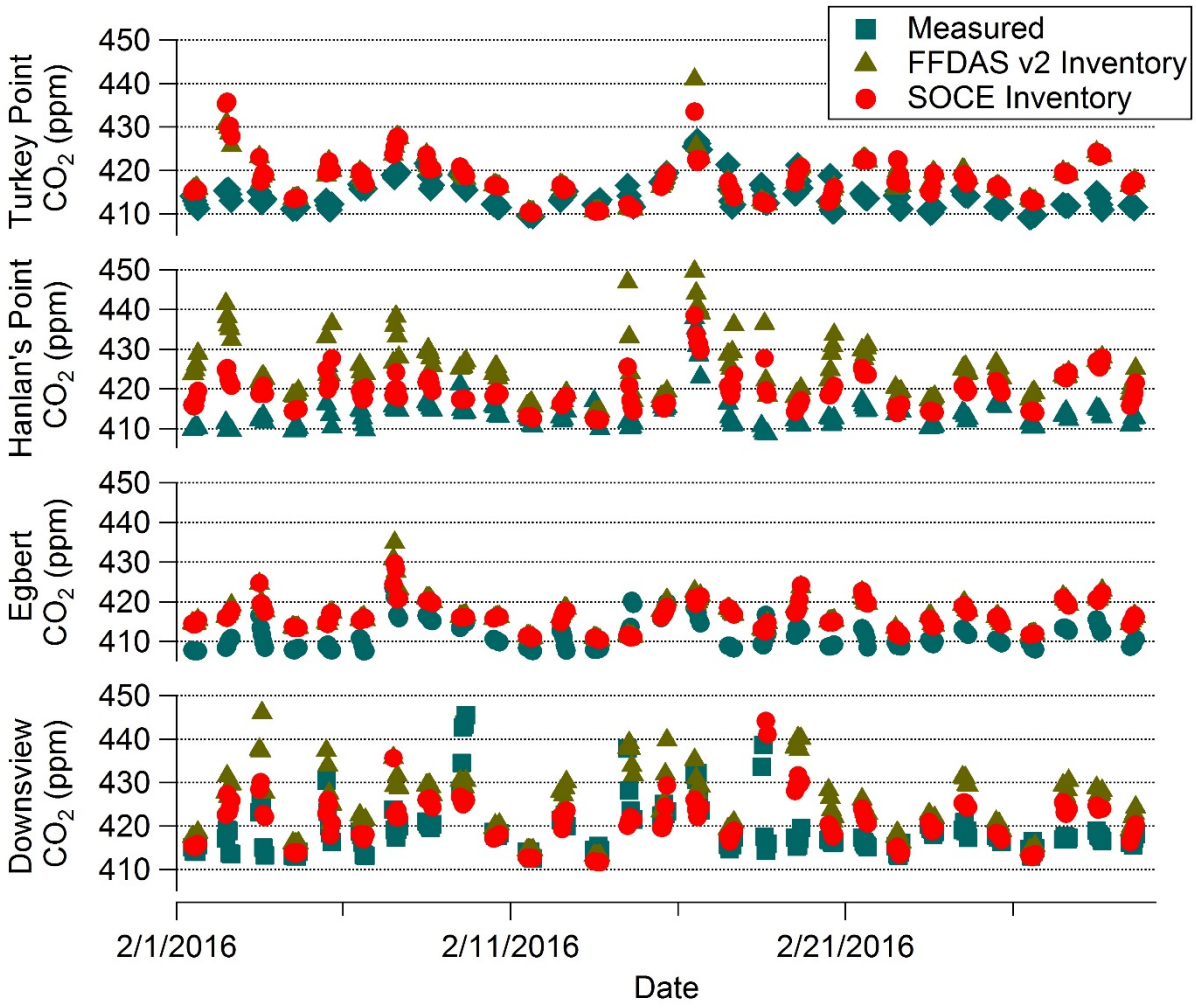

806

807 **Figure 4: Time series of measured (blue) and modelled February afternoon (12:00-16:00**
808 **EST) CO_2 mixing ratios for the four sites used in this study. The red and gold markers are the**
809 **modelled mixing ratios when using the SOCE CO_2 inventory and the FFDAS v2 inventory,**
810 **respectively.**

811

812

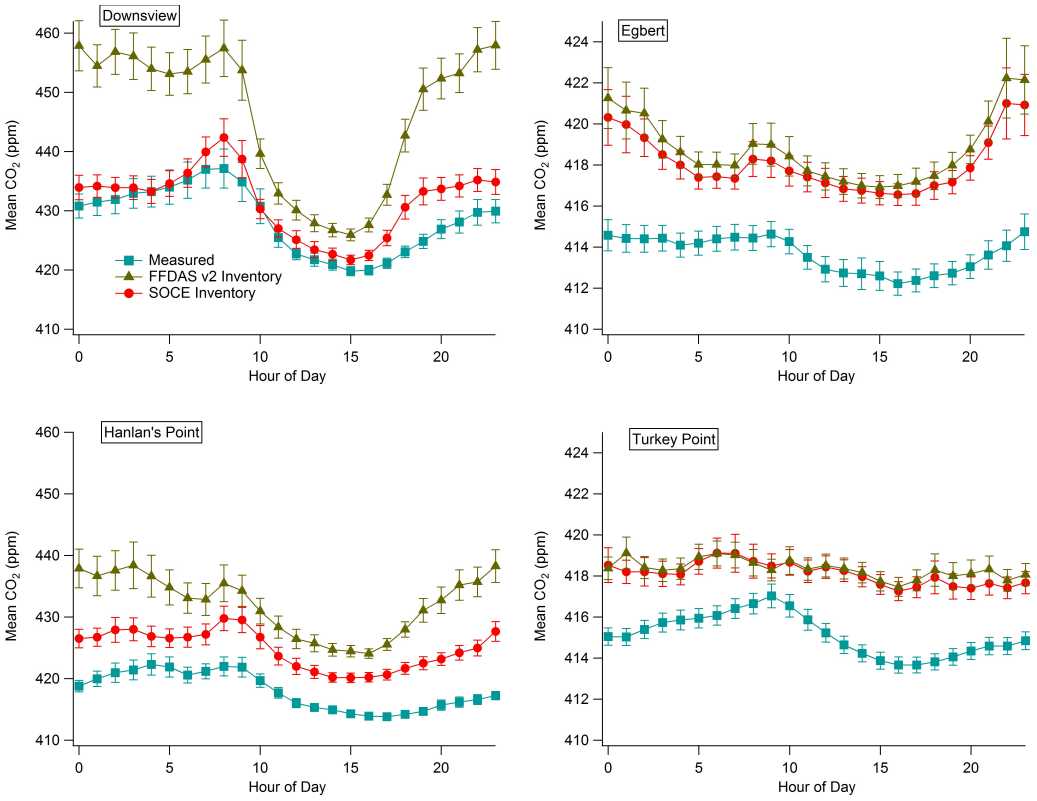

813

814

815 **Figure 5: Time series of mean measured (blue) and modelled diurnal CO_2 mixing ratios at**
816 **the four sites considered in this study for January – March 2016. The red and gold markers**
817 **are the modelled diurnal mixing ratios when using the SOCE CO_2 inventory and the FFDAS v2**
818 **inventory, respectively. Note the difference in scale for urban and rural sites. Error bars**
819 **represent standard error of the mean.**

820

821

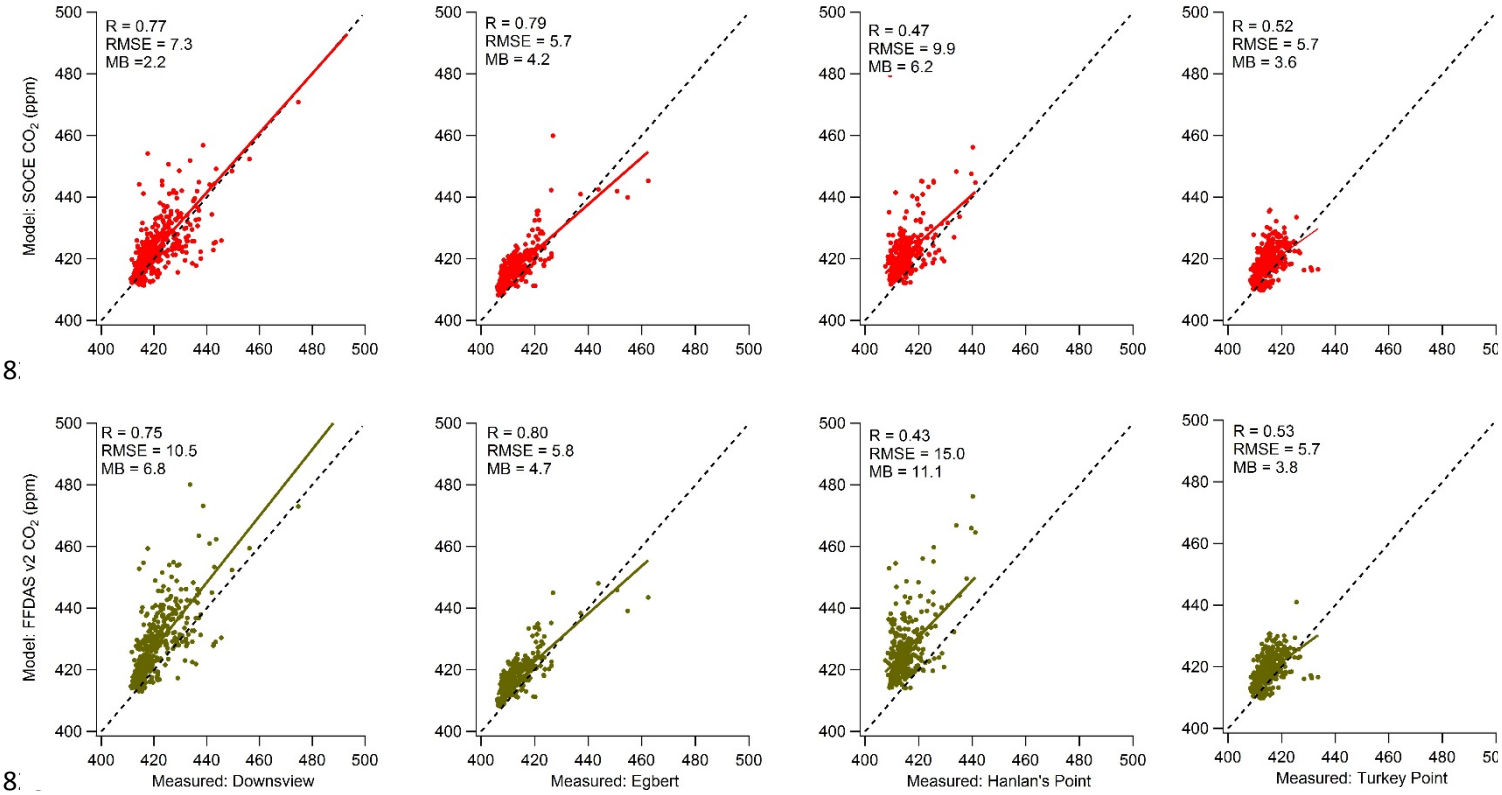

Figure 6: Scatter plot of the modelled and measured afternoon (12:00-16:00 EST) CO_2 mixing ratios from January-March, 2016 at the four monitoring stations used in this study. The top and bottom panels show measurement-model correlation when the SOCE inventory and the FFDAS v2 inventory were used, respectively. The model vs. measurement Correlation Coefficient (R), root mean square error (RMSE) and mean bias (MB) (units: ppm) are provided within each panel. Solid lines are the standard major axis regression lines and dashed lines are 1:1 lines shown for reference.

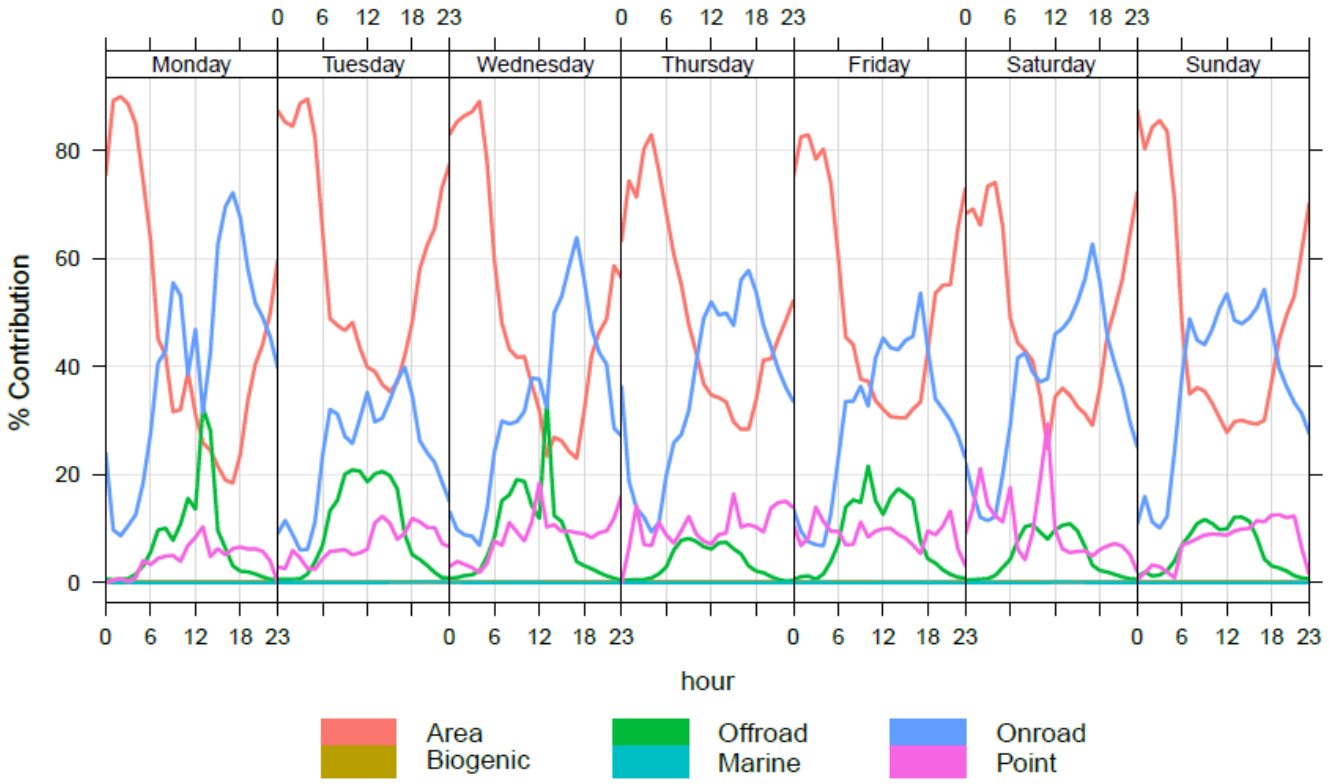

832

833

834 **Figure 7: Modelled sectoral percent contributions to diurnal local CO_2 enhancement for**
835 **February 2016 at Downsview averaged by day of week. Note: Area = Area + Residential**
836 **natural gas combustion + Commercial natural gas combustion. (Time zone is EST).**

837